Citrate-Coated Gold Nanoparticles As Smart Scavengers for Mercury(II) Removal from Polluted Waters

ARTICLE *in* ACS NANO · FEBRUARY 2012

Impact Factor: 12.88 · DOI: 10.1021/nn204313a · Source: PubMed

4 AUTHORS:

Isaac Ojea Jimenez
European Commission
38 PUBLICATIONS **567** CITATIONS
SEE PROFILE

Lopez Xicotencatl
Universidad Nacional Autónoma de México
3 PUBLICATIONS **58** CITATIONS
SEE PROFILE

Jordi Arbiol
Catalan Institute of Nanoscience and Nanot…
347 PUBLICATIONS **7,605** CITATIONS
SEE PROFILE

Victor Puntes
Catalan Institute of Nanoscience and Nanot…
129 PUBLICATIONS **7,101** CITATIONS
SEE PROFILE

Citrate-Coated Gold Nanoparticles As Smart Scavengers for Mercury(II) Removal from Polluted Waters

Isaac Ojea-Jiménez,[†,*] Xicoténcatl López,[†,‡] Jordi Arbiol,[§,⊥] and Victor Puntes[†,⊥,*]

[†]Institut Català de Nanotecnologia (ICN), Campus UAB, 08193, Cerdanyola del Vallés, Spain, [§]Institut de Ciència de Materials de Barcelona (ICMAB-CSIC), Campus UAB, 08193, Cerdanyola del Vallés, Spain, and [⊥]Institució Catalana de Recerca i Estudis Avançats (ICREA), 08093, Barcelona, Spain. [‡]Present address: Centro de Física Aplicada y Tecnología Avanzada, Universidad Nacional Autónoma de México, Querétaro, México.

ABSTRACT Colloidal gold nanoparticles (Au NPs) have been employed as single entities for rapid scanning and sequestration of Hg(II) from multicomponent aqueous solutions containing low pollutant concentrations. Under the studied conditions, sodium citrate has been identified as the reducing agent and Au NPs as the catalyst in the reduction of Hg(II), which is efficiently trapped in the presence of other cations such as Cu(II) and Fe(III). The effect of Hg(II) uptake implies amalgam formation, which leads to remarkable morphological transformations. The hydrophobicity of the resulting amalgam and consequent expulsion from water eases its recovery. The interaction between Au and Hg has been studied using UV–vis, ICP-MS, (S)TEM, SEM, EDX, and XRD.

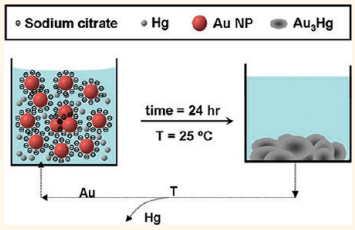

KEYWORDS: gold nanoparticles · mercury removal · amalgam · wastewater · citrate reducer · catalysis

More than two centuries after the industrial revolution, the world is facing formidable challenges meeting rising demands of potable water. The available supplies of freshwater are decreasing due to extended droughts, population growth, and increasing groundwater and environmental pollution. Among the most notorious pollutants, mercury is a highly toxic heavy metal present in the environment and has been reported to cause permanent harmful effects in living organisms at relatively low dose, such as memory loss, neuronal, hepatic, and nephritic damage, decrease in the rate of fertility, as well as birth defects in offspring.[1] Natural sources of contamination by mercury are volcanic eruptions and mercury-rich soils, containing an average of 80 ppb of Hg, whose eluviations contribute to its accumulation in water streams. The major anthropogenic sources basically include industrial waste, mining, pharmaceutical and pesticide products, and processing and refining of mercury ores.[2] For example, the United States Environmental Protection Agency (US-EPA) estimates that coal-fired utility commercial boilers emit 50–55 tons of total mercury per year in the U.S.[3] Hg(II) constitutes the majority of mercury in the hydrosphere and is the predominant form in aqueous phase. Most of the remediation technologies available today, which are based on the adsorption,[4–6] ion exchange,[3,7,8] amalgamation,[9,10] or chemical precipitation[11] of mercury, while effective, very often are costly and time-consuming, particularly pump-and-treat methods that require costly investments and procedures. Some additional challenges are the ability to remove *in situ* toxic compounds from subsurface and other environments that are difficult to access and the capacity to clean extremely low concentrations of pollutants but still under the threshold of safety.

Advances in nanoscale science and engineering are providing new opportunities to develop more cost-effective and environmentally acceptable water purification processes. Nanomaterials have a number of physicochemical properties that make them particularly attractive for water purification such as higher surface area per unit volume and the ability to be functionalized with a number of surfactants to enhance their affinity toward target molecules, such as in the case of dimercaptosuccinic acid-coated magnetite NPs, where the thiolated ligand acts as an effective sorbent for toxic soft metals such as Hg, Ag, Pb, Cd, and Tl.[12] Due to their reduced size and high curvature radii, the surface is especially reactive (mainly due to the high density of low coordinated atoms at the surface, edges, and corners). In addition, for certain reduced diameters, NPs are sustained by Brownian dispersion, avoiding sedimentation, so they can be maintained by exploring the volume without agitation.

* Address correspondence to isaac.ojea@icn.cat; victor.puntes@icn.cat.

Received for review November 7, 2011 and accepted February 14, 2012.

Published online February 14, 2012
10.1021/nn204313a

This capacity to be dispersed in groundwater allows them to travel farther than larger macro-sized particles, thus achieving a wider distribution and permitting the whole volume to be quickly scanned with a relatively low number of particles.[13−15] For example, in a rough estimation, a 10 nm metallic NP in water at room temperature (RT) will experience Brownian relaxation on the order of a nanosecond, and after each Brownian step in solution it will move about 10 to 20 nm.[16] Therefore, a typical NP concentration of a few nanomolars will explore the total volume in about a centisecond (assuming a 10% efficiency; *i.e.*, the NP would, on average, repeat previous positions up to 10 times before visiting a new one).

The high adsorption capacity of nanomaterials for certain pollutants has been demonstrated in many cases. For example, heavy metals have been effectively removed from contaminated water, as in the cases of Cr(VI) employing maghemite NPs,[17] Cr(III) with silica NPs,[18] or Hg(II) with alumina NPs.[19] In addition, the magnetic properties of iron oxide NPs have been employed for the elimination of As(III) and As(V) from drinking water supplies, which involves the formation of weak arsenic−iron oxide complexes at the NP surface.[20,21] Alternatively, specific functionalization can also be used on semiconductor systems to trap organic molecules and then promote their complete degradation making use of the photocatalytic properties.[22] A comprehensive overview of the different manufactured nanomaterials along with the pollutants they could potentially remediate has been reviewed elsewhere.[14]

Gold amalgam, an alloy spontaneously formed by the reaction of mercury with gold, had been conventionally produced during 19th century placer mining, when large amounts of mercury were used for gold extraction from ore. In the present work, we investigate the reverse approach, which employs gold to remove mercury from water. The interaction between gold and mercury requires the presence of the reduced form of mercury, Hg(0), so that a weak reducing agent in combination with metallic Au NPs is needed to produce the final amalgam. In our case, the sodium citrate ions coating the NPs act as a reducing agent of Hg(II) catalyzed by the Au atoms on the surface, thus avoiding the use of $NaBH_4$, a toxic and nonspecific (too strong) reducing agent. In fact, this strategy is used to grow large Au NPs or Au nanorods using CTAB and ascorbic acid. The amalgamation/elimination process causes Au NPs to evolve into nonspherical coalescent NPs of increasing size, which are then expulsed from the solution. The novelty of this work not only resides in the description of a chemical process but also includes the ability of Au NPs to search, reduce, and trap mercury from water in a selective manner. The recent publication of Mertens *et al*. highlights that the topic raises interest from a broad scientific community and at the same time complements our observations.[23]

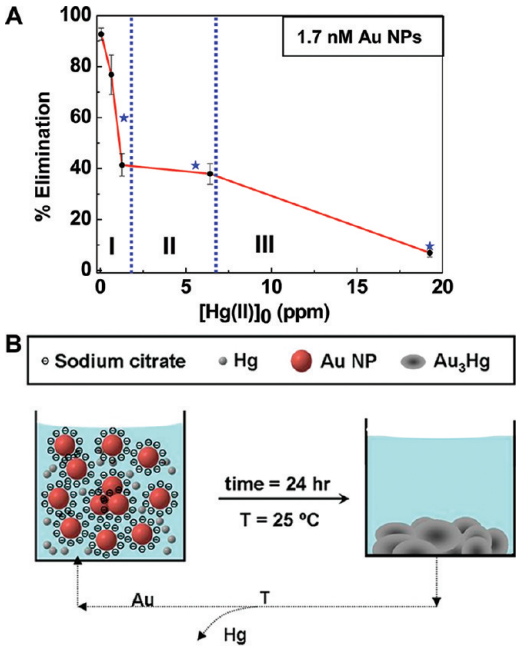

Figure 1. Removal of Hg by Au NPs from water solutions. (A) Percentage of elimination of Hg(II) employing a constant Au NP concentration (1.7 nM Au NPs, 7.1 ppm Au) from samples containing increasing initial $HgCl_2$ concentrations in Milli-Q water (circles with error bars) or in river water (stars). All the concentrations refer to the total amount in the reaction vessel. (B) Schematic representation of the Hg(II) elimination process through amalgam formation (not drawn to scale). The recovery of Hg and Au from the amalgam is a well-known and extended process.

RESULTS AND DISCUSSION

Removal of Mercury. We decided to employ relatively small Au NPs (8.9 ± 1.6 nm) as a model for these studies due to their simple preparation procedure by the citrate-reduction method[24] and given the large number of atoms present at the surface of NPs of this size (*ca*. 26% of total atoms on the surface).[25] As expected, the decrease of Au NP size has been reported to increase mercury removal.[26,27] In order to study the absorption, we performed several experiments by mixing a colloidal Au NP solution with samples of increasing initial concentrations of $HgCl_2$ in Milli-Q water (Figure 1). From ICP-MS analysis of reacted samples at 48 h (a time large enough to saturate the Au NPs), there could be observed three different regimes regarding the percentage of eliminated Hg(II) *vs* initial $[Hg(II)]_0$: (i) a first pronounced drop for $[Hg(II)]_0$ from 0.065 to 1.28 ppm, (ii) a less marked removal ratio up to $[Hg(II)]_0 = 6.5$ ppm, and (iii) a low percentage of elimination for $[Hg(II)]_0 > 6.5$ ppm. The first two regimes could be correlated with the different reported modes of surface interaction between Au and Hg,[28,29] which are the chemisorption of Hg(II) on the surface of the Au NPs and amalgam formation. These will be further discussed after we examine the samples by HRTEM, EDX, and XRD analyses later in this article. The third regime, at high $[Hg(II)]_0 > 6.5$ ppm, is a consequence of the excess

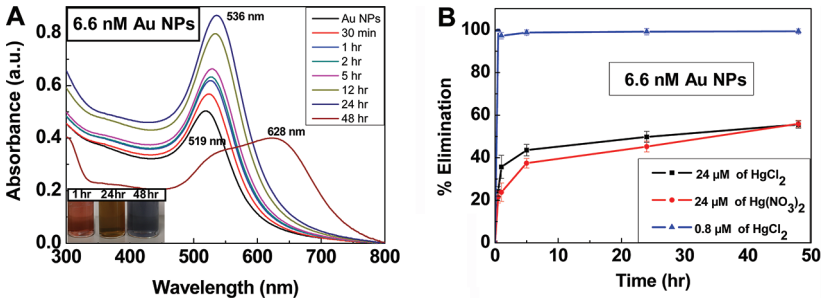

Figure 2. Optical evolution of the removal process. (A) UV−vis absorption spectra of Au NP samples (6.6 nM Au NPs, 28.4 ppm Au) collected at different time intervals in a batch reaction containing a total [$HgCl_2$] = 320 μM (64 ppm Hg). (Inset) Images corresponding to the interaction process between Au and Hg after different periods of time. (B) Time evolution of elimination of mercury with Au NPs (6.6 nM Au NPs, 28.4 ppm Au) from samples containing [$HgCl_2$] = [$Hg(NO_3)_2$] = 24 μM (4.8 ppm Hg) and [$HgCl_2$] = 0.8 μM (0.16 ppm Hg). All the concentrations refer to the total amount in the reaction vessel.

of Hg(II) and saturation of the available Au NPs surface. The observed uptake capacity is approximately 0.4 mg of Hg(II) per mg of Au, which is above the previously reported value using Au NPs supported on alumina.[27] Regarding the atomic percent of Hg from the total mass (which in our case is 33%), it is very close to the limit of incorporation into Au (*ca.* 27% at room temperature) when it transforms into the stable amalgam Au_3Hg, as can be seen from the corresponding Hg−Au phase diagram.[30]

The UV−vis absorption spectrum of Au NPs is very sensitive to variations of the chemical environment at the NP surface. We monitored the surface plasmon resonance peak of Au NPs as a function of time immediately after mixing a colloidal Au NP solution with a solution of $HgCl_2$ in Milli-Q water (Figure 2). Note that the initial concentrations of Au NPs and Hg(II) were increased with respect to experiments in Figure 1 (from 1.7 to 6.6 nM) in order to better appreciate changes in the absorption spectra. UV−vis spectroscopy revealed a progressive red-shift of the absorption band from 519 to 536 nm during the first 24 h and then a drop in intensity together with a peak broadening and shifting to 628 nm after 48 h. This shift in the peak position is indicative of a strong variation of the NPs morphology,[29] which already suggests some kind of deposition of mercury on the Au NP surface followed by aggregation.[27,28] As can be observed from the colors of the solutions (Figure 2A, inset), at short times (less than 24 h) the initial red color of the Au NPs solution became progressively more orange-brown due to increasing mercury incorporation,[28] whereas longer exposures caused aggregation of the Au NPs and the appearance of a blue color.

Upon varying the Hg(II) source and monitoring its removal with time, ICP-MS analysis of the supernatant revealed that Au NPs (6.6 nM of NPs, 28.4 ppm Au) were able to remove Hg(II) to the extent that they capture up to 58% of the total Hg ions available in solutions containing 24 μM (4.8 ppm) of Hg [added either in the form of $HgCl_2$ or as $Hg(NO_3)_2$] (Figure 2B). Furthermore, for a 0.8 μM $HgCl_2$ solution containing 0.16 ppm Hg(II) ions, the removal was 100%. Note that all three reactions afforded more than the 70% of their ion removal capacity in less than 5 h.

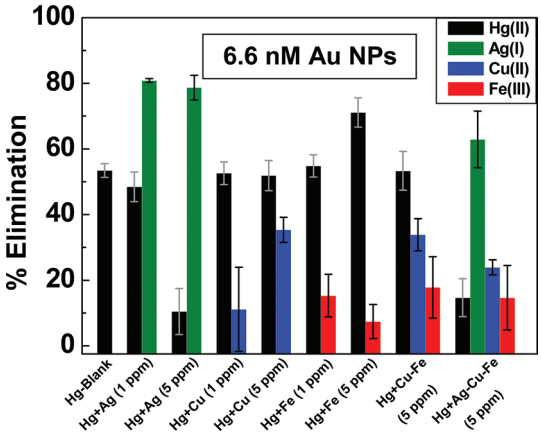

Figure 3. Selective Hg removal in the presence of added cations Ag(I), Cu(II) and Fe(III). Elimination of mercury with Au NPs (6.6 nM Au NPs, 28.4 ppm Au) from samples containing [$HgCl_2$] = 24 μM (4.8 ppm Hg) and either $AgNO_3$ (1 or 5 ppm), $CuSO_4$ (1 or 5 ppm Cu), $FeCl_3$ (1 or 5 ppm Fe), or mixtures of either $CuSO_4$ and $FeCl_3$ (5 ppm each cation) or $AgNO_3$, $CuSO_4$, and $FeCl_3$ (5 ppm each cation). All concentrations refer to the total amount in the reaction vessel.

The ability of the Au NPs to trap cations is related to their catalytic reduction and alloy formation properties. The adsorption capacity of Au NPs was tested in the presence of other cations, *i.e.*, Ag(I) [Ag(I)/Ag(0), E^0 = 0.80 V], Cu(II) [Cu(II)/Cu(0), E^0 = 0.34 V], and Fe(III) [Fe(III)/Fe(0), E^0 = 0.037 V], with different reduction potentials [Hg(II)/Hg(0), E^0 = 0.85 V] and affinity for gold (Ag and Cu mix well with Au, while Fe does not, and Hg shows different AuHg phases). The experiments were performed under similar reaction conditions to before (*i.e.*, a solution of 6.6 nM Au NPs and 24 μM $HgCl_2$) in the presence of either $AgNO_3$, $CuSO_4$, or $FeCl_3$, considering two different concentrations of each cation (1 and 5 ppm) in the final solution (Figure 3). In addition, the effect of different mixtures of cations simultaneously present in the same reaction vessel was also analyzed, which consisted of either mixtures of Cu(II) and Fe(III) only or mixtures of all three cations. The results showed that the adsorption capacity of Au NPs toward mercury was maintained in all cases except when Ag(I) ions were present at 5 ppm

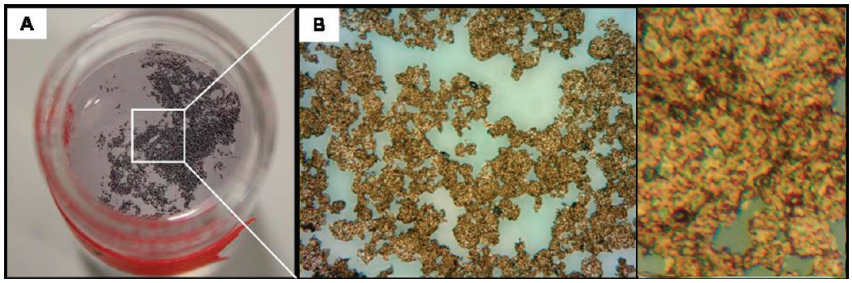

Figure 4. Removal of Hg from the Ebro River. (A) View of the precipitate resulting from the treatment of 6.5 ppm Hg(II) with Au NPs (1.7 nM Au NPs, 7.1 ppm Au) in Ebro River water (41% elimination). (B) Optical microscope image of the precipitate taken at 40× magnification and zoom.

concentration, which resulted in a proportional drop of the total Hg removal down to about 10%. This observation could be a consequence of the similar reduction potential between Hg(II) and Ag(I) and the higher miscibility of Au and Ag. Subsequently, the reduced silver ions could, in principle, either form a stable amalgam with mercury[31] or be adsorbed on the Au NPs surface.[32] The results shown in Figure 3 are more indicative of the second situation given the high levels of elimination of Ag(I) observed (~80%), thus significantly hampering the removal efficiency of Hg(II). Similarly, some degree of adsorption of Cu(II) and Fe(III) ions could also be observed (up to ~30% and ~20%, respectively) under the same reaction conditions. This selective elimination ability of Au NPs correlates very well with the different standard reduction potentials of the metals, with Fe(III) having the lowest value and being less prone to reduction. In addition, the moderate removal ratios observed for copper could also be explained by its ability to alloy with mercury and gold,[33] which contrasts with the case of iron, which does not form stable alloys at all.

The selectivity of Au NPs for Hg(II) was further evaluated in a more representative situation of natural wastewater such as that coming from a river after crossing an industrial area (Flix, Ebro River, Spain, Supporting Information, Table 1),[34] which contains not only a variety of dissolved cationic and anionic species but also organic matter in suspension. This multicomponent solution could interact with mercury to give a variety of its derivatives and/or with the Au NPs, poisoning and deactivating its surface. In this case, it was not necessary to precipitate the Au NPs by centrifugation or addition of NaCl since black aggregates were found both at the bottom of the reaction vessel and floating on the surface (that finally sedimented), together with a loss of the solution color observed after 24 h (Figure 4A). The floating aggregates are a consequence of the high hydrophobicity of the Au_3Hg amalgam. Analysis by ICP-MS revealed a similar percentage of eliminated Hg(II) to that in the experiments of Figure 1 (using 1.7 nM Au NPs, 7.1 ppm Au), where pure Milli-Q water was employed. Interestingly, optical microscope images of precipitated samples of the amalgam showed a typical shine and red color corresponding to nanometric and macroscopic forms of gold, respectively, with dark gray fringes emerging and connecting the amalgam material (Figure 4B).

Characterization of the Au−Hg System. Further analysis by TEM of samples collected at different times showed a dramatic evolution of the NP morphology upon interaction with Hg(II) (Figure 5). At initial times of less than 1 h, the Au NPs were spherical in shape and uniformly distributed, but later they evolved into nonspherical coalescent NPs of varying size, which suggests Au wetting and coalescence by mercury during the amalgamation process. Similar NP cementation has recently been observed between growing NPs[35] and in the incorporation of Hg(II) into CdTe or CdSe NPs.[36,37] From HAADF STEM micrographs of different areas of mercury-treated Au NPs it could be observed that most of the Au NPs were embedded into a mercury-rich matrix, which contributed to the fusion of the NPs and formed a continuous phase (Figure 6A and B). This is facilitated by the diffusivity of mercury in gold at room temperature, which is relatively high (estimated $D_{298} \approx 30\ \mu m^2/s$)[38] and likely enhanced at the nanoscale.[39] Additional EDX analysis yielded local molar ratios of Au:Hg ranging from 90:10 to 68:32 (atom %), corresponding to the micrographs of Figure 6A and B, respectively, which indicates that these bimetallic alloys are not equally distributed (Supporting Information, S1). This lack of uniformity could be explained by the presence of two different mechanisms of action: (i) surface covering of Au NPs by a mercury layer (chemisorption) and (ii) amalgamation between Au and Hg, which occurs to different extents depending on the reaction time, the ratio Au/Hg, and the surface area of the Au NPs available. HRTEM micrographs and the lattice resolved image of a section of the Au−Hg nanoparticle showed an interplanar distance of 2.24 Å, typical of the planes in the hexagonal close packed (hcp) Au_3Hg amalgam structure (Figure 6C). However, some of the NPs also exhibit a spacing of 2.35 Å corresponding to the (111) planes of the face-centered cubic (fcc) phase from pure Au NPs (Supporting Information, S2). These observations confirmed that some pure Hg is dispersed around the NPs, while the fcc Au phase can admit a certain amount of Hg before the crystal structure changes.[30] SEM images were also taken for a

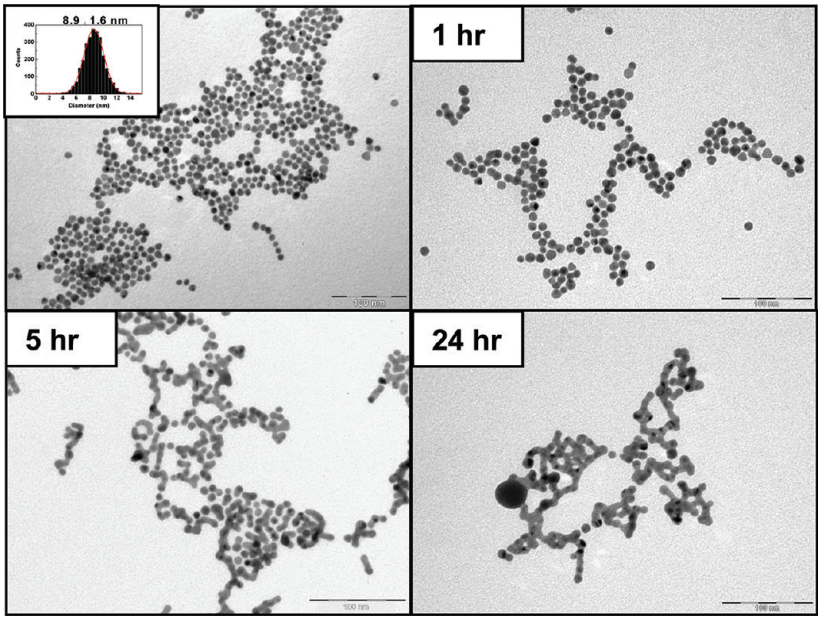

Figure 5. TEM images of Au NPs. As-synthesized (top left) and Au NPs samples (6.6 nM Au NPs, 28.4 ppm Au) collected at different times after treatment with 4.8 ppm Hg(II) in Milli-Q water.

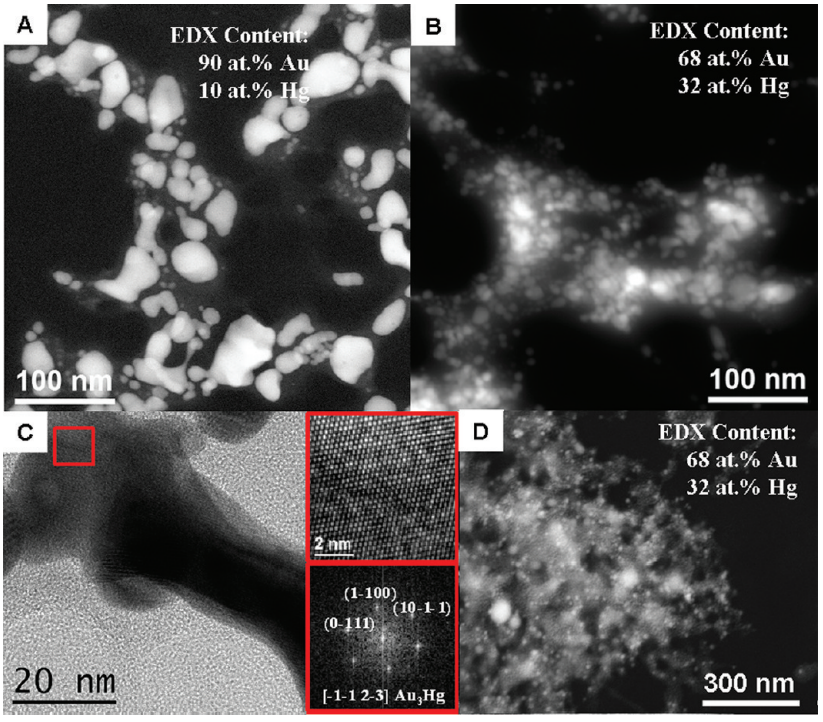

Figure 6. Electron microscopy images of the resulting Au–Hg system. (A and B) TEM HAADF STEM (Z-contrast) general views of different regions of Au NPs (6.6 nM Au NPs, 28.4 ppm Au) after treatment with 4.8 ppm Hg(II); (C) HRTEM analysis of the Au–Hg NPs with the corresponding lattice-resolved image of a section; (D) SEM backscattered electron image of the precipitated NPs. All the concentrations refer to the total amount in the reaction vessel.

better understanding of the morphology of Au NPs treated with Hg(II), which confirmed the presence of small particles embedded randomly into a matrix probably resulting from the amalgamation process (Figure 6D). The corresponding EDX spectrum of selected areas revealed a Au:Hg ratio of 68:31 (atomic %) (Supporting Information, S3), which is in agreement with the previous values obtained in the STEM mode. These results support the assumption of an oversaturation of the absorption capacity of Au and show the high ability of these NPs to interact with mercury.

The composite Au–Hg particles were further analyzed using XRD, showing the crystalline structure of Au NPs in the absence and in the presence of 4.8 ppm

Hg(II) after 1 and 24 h. The 2θ Bragg peaks obtained at 38.22°, 43.86°, 64.70°, 77.62°, and 81.68° (Figure 7) correspond to the (111), (200), (220), (311), and (222) Au fcc reflections, respectively.[40] The slight broadening and shift in the measured 2θ Bragg peaks of the mercury-treated Au NPs ($\sim$ 0.11° and $\sim$0.15° for 1 and 24 h treatment, respectively) indicate that there may be a compression of the Au crystal lattice due to the incorporation of Hg(0) to form the amalgam structure, which can be explained by Vegard's law. This demonstrates a change in the material while maintaining the overall cubic structure. The lattice parameters (*a*) of the Au NPs after 1 and 24 h treatment with 4.8 ppm Hg(II) (Figure 7B and C) were calculated to be 4.075 and 4.068 Å, respectively. Assuming a linear relationship between the lattice parameter and the relative Au and Hg concentrations in the nanocrystals, the presence of Hg in the amalgam was calculated to be 4.1% and 13.7%, respectively.[41] Interestingly, in the case of short reaction times (1 h), very narrow peaks at 31.67°, 45.44°, 66.19°, 75.24°, and 83.92° could also be observed, corresponding to (110), (200), (220), (112), and (202) reflections of large domains of tetragonal metallic Hg(0) (*I*4/*mmm*).[42] The presence of metallic Hg(0) confirms the reduction of Hg(II) at the NP surface before forming Hg−Au alloys. As the Au_3Hg alloy is thermodynamically favored at RT, with increasing time and mercury concentration the amount of amalgam increases. After 24 h, most of the reduced form of Hg(0) is incorporated into the Au NPs to form the amalgam structure Au_3Hg. This is in agreement with recent density functional theory (DFT) calculations, which demonstrated that the initial adsorption of mercury on the surface of Au NPs is a fast process, but that the inward metal interdiffusion is slow.[23] Evidently, the coalescence of amalgamated NPs causes a drastic reduction of the available Au NP surface and hampers the adsorption of more mercury.

According to the experimental observations, Hg(II) is eliminated by being reduced to its metallic form Hg(0), previously to the interaction with Au NPs. In principle, due to the noble nature of metallic Au [Au(III)/Au(0), E^0 = 1.51 V], one would not expect Hg(II) to oxidize Au(0) under standard conditions. Sodium citrate by itself was discarded as the reducing agent since no Hg(II) removal could be observed by ICP-MS analysis when the experiment of Figure 2B [using 4.8 ppm Hg(II)] was repeated with a solution of sodium citrate (2.2 mM) in the absence of Au NPs. In addition, no further Hg(II) elimination could be observed when the concentration of sodium citrate was increased 9-fold from the original one in the experiment of Figure 2B. Previous studies in the literature confirmed that sodium citrate has no reducing effect over Hg(II), although it showed a high capacity for complexation.[43] However, the presence of sodium citrate adsorbed on the surface of Au NPs could trigger a reduction

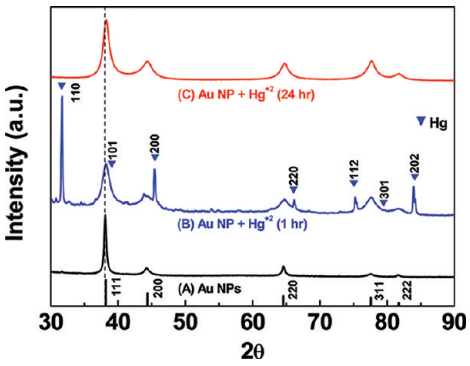

Figure 7. Cyrstal structure of Au NPs before and after Hg uptake. XRD pattern of Au NPs (6.6 nM Au NPs, 28.4 ppm Au) treated with 4.8 ppm Hg(II). The triangles represent reference values of tetragonal Hg (*I*4/*mmm*), and the cubic Au (*Fm*3*m*) values are shown on the *x*-axis.

mechanism catalyzed by the very reactive Au surface atoms, in a similar way to what has been postulated for the disproportionation of Hg(I).[28] Such an assumption was confirmed when differently coated Au NPs (*i.e.*, 11-mercaptoundecanoic acid or amino polyethylene glycol-MW 1000), after proper purification of sodium citrate and the excess of ligands by dialysis, were employed for the treatment of a solution of $HgCl_2$ under the same reaction conditions used before. In these particular cases, where the sodium citrate was first displaced from the surface of the Au NPs and then cleaned from the solution, no mercury removal could be observed at all after more than 48 h of reaction. These results confirmed that there exists a combined role of sodium citrate as the coating and reducing agent and Au NPs as the catalyst in the adsorption/amalgamation process of Hg(II).

CONCLUSIONS

We have demonstrated the ability of Au NPs to be used for the elimination of Hg(II) from both Milli-Q water and real water. The process involves chemisorption of Hg(II), reduction, precipitation on the top of the NP, and the consequent metal interdiffusion and alloying.[33] The final product is a mixture of Au_3Hg alloy together with other areas richer in either Au or Hg. As Hg grows on top of the Au NPs, the available surface decreases until the reaction stops.

Despite the price of gold, the efficiency of the process and the ability of its easy recovery can make the whole process viable, especially in closed environments such as wastewater treatment plants. In principle, the purification would be carried out in closed water reservoirs (batch conditions) and the NPs amalgamated and sedimented by this process. An advantage would be that Au can then be recovered by exposing the amalgam to a high pressure or temperature[42] and the Hg disposed of (see Supporting Information for an estimation of the expected material and recovery costs and comparison of cost with other

removal methods, S4). Due to increasing environmental awareness and stricter regulations on acceptable levels of mercury emissions, at the present moment there is a great interest in removing mercury from streams containing relatively low concentrations (Hg < 100 ppb).[44] Although the method described here is majorly efficient for initial concentrations of Hg(II) < 1 ppm, it must be emphasized that we managed to reduce the amounts of Hg(II) from samples containing 65 ppb of $HgCl_2$ down to the levels for mercury in drinking water set by the World Health Organization (WHO) (*i.e.*, 1−5 ppb).[45] In addition to the good elimination ratio, our method avoids the previous limitation of introducing an additional reagent, such as $NaBH_4$, into water before the treatment. Finally, as Au nanoparticles can rapidly scan the whole volume, one can envisage the implementation of this method in a continuous flow.

EXPERIMENTAL SECTION

Chemicals. Mercury(II) chloride, mercury(II) nitrate monohydrate, sodium citrate, and gold(III) chloride trihydrate were purchased from Sigma-Aldrich and used as received without further purification. All glassware used was borosilicate glass and was washed with HNO_3 (15% in water) and rinsed three times with distilled Milli-Q water prior to use. Two stock solutions of Hg(II) (1.6 mM) were prepared by dissolving $HgCl_2$ and $Hg(NO_3)_2 \cdot H_2O$ into distilled water (43 and 55 mg in 100 mL of distilled water, respectively). Solutions were stored in a refrigerator (+4 °C). River water was taken from the Ebro River in Flix (Spain) and used directly without any further purification.

Instrumentation. Low-magnification transmission electron microscopy (TEM) analysis was performed on a JEOL1010 transmission electron microscope at an accelerating voltage of 80 kV. High-resolution (HR) TEM was performed on a JEOL2010F field emission gun microscope operated at 200 kV. High angular annular dark field (HAADF) and scanning TEM (STEM) were obtained on a JEOL2100 operated at 200 kV equipped with an energy-dispersive X-ray spectroscopy (EDX) detector. The sample (10 μL) was drop-cast onto ultrathin Formvar-coated 200-mesh copper grids (Tedpella, Inc.) and left to dry in air. For each sample, the size of 200 particles was measured to obtain the average and the size distribution. UV−vis absorption spectra were recorded with a Shimadzu UV-2401PC spectrophotometer at room temperature. Mercury analyses were performed using an inductively coupled plasma mass spectrometry (ICP-MS) Agilent instrument (model 7500cx) with a detection limit of 0.02386 ppb. Aliquots of the samples were diluted to an optimal concentration for ICP-MS analysis. Ga was used as the internal standard, and the integration time/point and time/mass were 0.1 and 0.3 s, respectively, with a 3× repetition. Scanning electron microscope (SEM) images and EDX studies were done in a FEI QUANTA-200 ESEM-FEG operating at an acceleration voltage of 20 kV. Samples were prepared by evaporating a drop of the reacted solution on top of a carbon support. Optic microscopy images of the precipitates were taken with an Axio Observer Z1m from Carl Zeiss. X-ray diffraction (XRD) data were collected on a PANalytical X'Pert diffractometer using a Cu Kα radiation source (λ = 1.5418 Å). In a typical experiment, the 2θ diffraction (Bragg) angles were measured by scanning the goniometer from 20° to 90° at a speed of 0.0014 s^{-1}. Samples were prepared by precipitating the particles by addition of NaCl and centrifugation (7000 rcf, 15 min) and smeared onto (510) off-axis silicon wafers (Silicon Materials).

Synthesis of Au NPs. Citrate-stabilized monodispersed Au NPs (5×10^{12} NPs/mL, 8.3 nM Au NPs, 35 ppm Au) were prepared based on the standard sodium citrate reducing methodology described in the literature for obtaining Au NPs.[24] In brief, sodium citrate (2.2 mM) was dissolved in H_2O (150 mL) in a three-neck round-bottom flask and heated to 100 °C. A solution of $HAuCl_4 \cdot 3H_2O$ (1 mL, 25 mM) in H_2O was injected, and the reaction mixture was maintained at the boiling temperature for a further 3.5 min before allowing it to cool to RT. The resulting Au NPs of 8.9 ± 1.6 nm (SD ≈ 16%) were characterized by UV−vis and TEM (Supporting Information, S1).

Removal of Mercury from Samples with Increasing Amounts of Hg(II-). Samples were prepared by mixing 2 mL of as-synthesized Au NP solution with 8 mL of different stock solutions of $HgCl_2$ (0.12, 0.04, 0.008, 0.004, and 0.0004 mM) in Milli-Q water at RT under stirring for 48 h. Aliquots (1 mL) were taken, precipitated with NaCl (10 mg), and centrifuged (22 °C, 12 000 rcf for 25 min), and the supernatant was collected for ICP-MS analysis. Each experiment was performed in triplicate. Similarly, experiments with river water were performed by mixing 2 mL of as-synthesized Au NP solution with 8 mL of stock solutions of $HgCl_2$ (0.12, 0.035, 0.0087 mM) in river water at RT under stirring for 24 h. Samples were centrifuged (22 °C, 12 000 rcf for 25 min), and the supernatant was collected for ICP-MS analysis.

UV−Vis Monitoring Experiments. The surface plasmon resonance peak of Au NPs was recorded as a function of time immediately after mixing 8 mL of as-synthesized Au NP solution and 2 mL of stock solution of 1.6 mM $HgCl_2$. The mixtures were continuously stirred at RT before aliquots were taken at different times (30 min, 1 h, 2 h, 5 h, 12 h, 24 h, and 48 h) and analyzed by UV−vis spectroscopy.

Time Evolution of Elimination of Hg. Samples were prepared by mixing 8 mL of as-synthesized Au NP solution with 2 mL of different stock solutions of Hg(II): 0.12 mM $HgCl_2$, 0.12 mM $Hg(NO_3)_2$, and 0.004 mM $HgCl_2$ in Milli-Q water at RT under stirring. Samples at different times (1, 5, and 24 h) were collected for TEM analysis. Aliquots (1 mL) were taken at different times (1, 2, 5, 24, and 48 h), NPs were precipitated with NaCl (10 mg), centrifuged (22 °C, 12 000 rcf for 25 min), and the supernatant was collected for ICP-MS analysis. Each experiment was performed in triplicate. Samples for XRD analyses were prepared under the same reaction conditions (using the 0.12 mM $HgCl_2$ stock solution) but employing 8-fold increased volumes of stock solutions. In this scaled-up experiment the degree of Hg removal was consistent with previous result and reproducible.

Selective Hg Removal in the Presence of Added Cations Ag(I), Cu(II), and Fe(III). Depending on the cation and the concentration required, a volume of 0.2 mL of stock solutions of $AgNO_3$ (0.5 and 2.4 mM), $CuSO_4$ (0.8 and 4 mM), and/or $FeCl_3$ (0.9 and 4.6 mM) in Milli-Q water was mixed with 2 mL of a stock solution of 0.12 mM $HgCl_2$. Samples were left to equilibrate at RT for 15 min before 8 mL of as-synthesized Au NP solution was added followed by further stirring for 48 h. Aliquots (1 mL) were taken, the NPs were precipitated with NaCl (10 mg) and centrifuged (22 °C, 12 000 rcf for 25 min), and the supernatant was collected for ICP-MS analysis. Each experiment was performed in triplicate.

Conflict of Interest: The authors declare no competing financial interest.

Acknowledgment. The authors thank Aleix Conesa and Beatriz Guerrero from Leitat Technological Center for ICP-MS analyses, Judith Oró-Solé from ICMAB for SEM characterization, David Casas from Programa Joves i Ciència de CatalunyaCaixa for help in the experimental work, and SCT-UB for the use of their (S)TEM equipment.

Supporting Information Available: Physicochemical parameters of Ebro River water, EDX analyses, HRTEM analyses, SEM analyses, and images. This material is available free of charge *via* the Internet at http://pubs.acs.org.

REFERENCES AND NOTES

1. Zahir, F.; Rizwi, S. J.; Haq, S. K.; Khan, R. H. Low Dose Mercury Toxicity and Human Health. *Environ. Tox. Pharm.* **2005**, *20*, 351–360.

2. Lin, C.-J.; Pehkonen, S. O. The Chemistry of Atmospheric Mercury: A Review. *Atmos. Environ.* **1999**, *33*, 2067–2079.
3. Kudlac, G. A.; Amrheim, G. T. In *Enhanced Mercury Control for Coal-Fired Utility Boilers*, 7th Annual Pittsburgh Coal Conference, Pittsburgh, PA, 2000.
4. Evangelista, S. M.; DeOliveira, E.; Castro, G. R.; Zara, L. F.; Prado, A. G. S. Hexagonal Mesoporous Silica Modified with 2-Mercaptothiazoline for Removing Mercury from Water Solution. *Surf. Sci.* **2007**, *601*, 2194–2202.
5. Olkhovyk, O.; Jaroniec, M. Ordered Mesoporous Silicas with 2,5-Dimercapto-1,3,4-thiadiazole Ligand: High Capacity Adsorbents for Mercury Ions. *Adsorption* **2005**, *11*, 205–214.
6. Park, H. G.; Kim, T. W.; Chae, M. Y.; Yoo, I.-K. Activated Carbon-Containing Alginate Adsorbent for the Simultaneous Removal of Heavy Metals and Toxic Organics. *Proc. Biochem.* **2007**, *42*, 1371–1377.
7. Chiarle, S.; Ratto, M.; Rovatti, M. Mercury Removal from Water by Ion Exchange Resins Adsorption. *Water Res.* **2000**, *34*, 2971–2978.
8. Ritter, J. A.; Bibler, J. P. Removal of Mercury from Waste Water: Large-Scale Performance of an Ion Exchange Process. *Water Sci. Technol.* **1992**, *25*, 165–172.
9. Biester, H.; Schuhmacher, P.; Müller, G. Effectiveness of Mossy Tin Filters to Remove Mercury from Aqueous Solution by Hg(II) Reduction and Hg(0) Amalgamation. *Water Res.* **2000**, *34*, 2031–2036.
10. Huttenloch, P.; Roehl, K. E.; Czurda, K. Use of Copper Shavings To Remove Mercury from Contaminated Groundwater or Wastewater by Amalgamation. *Environ. Sci. Technol.* **2003**, *37*, 4269–4273.
11. Kostal, J.; Mulchandani, A.; Gropp, K. E.; Chen, W. A Temperature Responsive Biopolymer for Mercury Remediation. *Environ. Sci. Technol.* **2003**, *37*, 4457–4462.
12. Yantasee, W.; Warner, C. L.; Sangvanich, T.; Addleman, R. S.; Carter, T. G.; Wiacek, R. J.; Fryxell, G. E.; Timchalk, C.; Warner, M. G. Removal of Heavy Metals from Aqueous Systems with Thiol Functionalized Superparamagnetic Nanoparticles. *Environ. Sci. Technol.* **2007**, *41*, 5114–5119.
13. Diallo, M. S.; Savage, N. Nanoparticles and Water Quality. *J. Nanopart. Res.* **2005**, *7*, 325–330.
14. Karn, B.; Kuiken, T.; Otto, M. Nanotechnology and in Situ Remediation: A Review of the Benefits and Potential Risks. *Environ. Health Perspect.* **2009**, *117*, 1813–1831.
15. Savage, N.; Diallo, M. S. Nanomaterials and Water Purification: Opportunities and Challenges. *J. Nanopart. Res.* **2005**, *7*, 331–342.
16. For a concentration of 10^{12} NP/mL, each NP must scan a volume that is *ca.* $1/10^{12}$ mL (10^9 nm^3). Since the volume of a 10 nm AuNP is 523 nm^3, each particle has to make 10^9/523 steps to visit its whole corresponding volume, which is about 1.91×10^6 steps. Finally, a 10% efficiency requires 10^7 steps, each of them taking 1 ns, which results that every 10^{-2} seconds the whole volume is explored.
17. Hu, J.; Chen, G.; Lo, I. M. C. Removal and Recovery of Cr(VI) from Wastewater by Maghemite Nanoparticles. *Water Res.* **2005**, *39*, 4528–4536.
18. Lopez, X.; Castaño, V. M. Chromium Removal from Industrial Water Through Functionallized Nanoparticles. *J. Nanosci. Nanotechnol.* **2009**, *8*, 5733–5738.
19. Pacheco, S.; Medina, M.; Valencia, F.; Tapia, J. Removal of Inorganic Mercury from Polluted Water Using Structured Nanoparticles. *J. Environ. Eng.* **2006**, *132*, 342–349.
20. Deliyanni, E. A.; Bakoyannakis, D. N.; Zouboulis, A. I.; Matis, K. A. Sorption of As(V) Ions by Akaganéite-type Nanocrystals. *Chemosphere* **2003**, *50*, 155–163.
21. Yavuz, C. T.; Mayo, J. T.; Yu, W. W.; Prakash, A.; Falkner, J. C.; Yean, S.; Cong, L.; Shipley, H. J.; Kan, A.; Tomson, M.; *et al.* Low-Field Magnetic Separation of Monodisperse Fe_3O_4 Nanocrystals. *Science* **2006**, *314*, 964–967.
22. Beydoun, D.; Amal, R.; Low, G.; McEvoy, S. Role of Nanoparticles in Photocatalysis. *J. Nanopart. Res.* **1999**, *1*, 439–458.
23. Mertens, S. F. L.; Gara, M.; Sologubenko, A. S.; Mayer, J.; Szidat, S.; Krämer, K. W.; Jacob, T.; Schiffrin, D. J.; Wandlowski, T. Au@Hg Nanoalloy Formation Through Direct Amalgamation: Structural, Spectroscopic, and Computational Evidence for Slow Nanoscale Diffusion. *Adv. Funct. Mater.* **2011**, *21*, 3259–3267.
24. Frens, G. Controlled Nucleation For Regulation of Particle-Size in Monodisperse Gold Suspensions. *Nat.-Phys. Sci.* **1973**, *241*, 20–22.
25. Assuming that the surface atoms form a spherical shell of thickness of d = 3 × Au atomic radius and that the percentage of surface atoms is in the same proportion as the shell's volume to the sphere's volume: $V_{shell}/V_{sphere} = (4/3)\pi(R^3 - (R - d)^3)/((4/3)\pi R^3) = (R^3 - (R - d)^3)/R^3$.
26. Mullett, M.; Tardio, J.; Bhargava, S.; Dobbs, C. Removal of Mercury from an Alumina Refinery Aqueous Stream. *J. Hazard. Mater.* **2007**, *144*, 274–282.
27. Lisha, K. P.; Anshup; Pradeep, T. Towards a Practical Solution for Removing Inorganic Mercury from Drinking Water Using Gold Nanoparticles. *Gold Bull.* **2009**, *42*, 144–a52.
28. Henglein, A.; Giersig, M. Optical and Chemical Observations on Gold-Mercury Nanoparticles in Aqueous Solution. *J. Phys. Chem. B* **2000**, *104*, 5056–5060.
29. Rex, M.; Hernandez, F. E.; Campiglia, A. D. Pushing the Limits of Mercury Sensors with Gold Nanorods. *Anal. Chem.* **2005**, *78*, 445–451.
30. Okamoto, H.; Massalski, T. The Au-Hg (Gold-Mercury) System. *J. Phase Equilib.* **1989**, *10*, 50–58.
31. Henglein, A.; Brancewicz, C. Absorption Spectra and Reactions of Colloidal Bimetallic Nanoparticles Containing Mercury. *Chem. Mater.* **1997**, *9*, 2164–2167.
32. Lou, T.; Chen, Z.; Wang, Y.; Chen, L. Blue-to-Red Colorimetric Sensing Strategy for Hg^{2+} and Ag^{+} *via* Redox-Regulated Surface Chemistry of Gold Nanoparticles. *ACS Appl. Mater. Interfaces* **2011**, *3*, 1568–1573.
33. Mori, H.; Komatsu, M.; Takeda, K.; Fujita, H. Spontaneous Alloying of Copper Into Gold Atom Clusters. *Philos. Mag. Lett.* **1991**, *63*, 173–178.
34. http://aca-web.gencat.cat/aca/appmanager/aca/aca/.
35. Lim, S. I.; Ojea-Jimenez, I.; Varon, M.; Casals, E.; Arbiol, J.; Puntes, V. Synthesis of Platinum Cubes, Polypods, Cuboctahedrons, and Raspberries Assisted by Cobalt Nanocrystals. *Nano Lett.* **2010**, *10*, 964–973.
36. Taniguchi, S.; Green, M. The Room-Temperature Structural and Optical Transformation of Cadmium Chalcogenide Quantum Dots Triggered by Reactive Cations. *J. Mater. Chem.* **2011**, *21*, 11592–11598.
37. Taniguchi, S.; Green, M.; Lim, T. The Room-Temperature Synthesis of Anisotropic CdHgTe Quantum Dot Alloys: A Molecular Welding Effect. *J. Am. Chem. Soc.* **2011**, *133*, 3328–3331.
38. Mortlock, A. J.; Rowe, A. H. Atomic Diffusion of Mercury in Gold. *Philos. Mag.* **1965**, *11*, 1157–1164.
39. Gonzalez, E.; Arbiol, J.; Puntes, V. Carving at the Nanoscale: Galvanic Replacement versus Kirkendall Effect at Room Temperature. *Science* **2011**, *334*, 1377–1380.
40. JCPDS card no. 04-0784.
41. The Au and Hg lattice parameters (*a*) used to calculate the % of Hg in Au NPs were 4.078 and 4.005 Å, respectively. The *a* for the body-centered tetragonal Hg was obtained from: Atoji, M.; Schirber, J. E.; Swenson, C. A. *J. Chem. Phys.* **1959**, *31*), 1628–1629.
42. Sneed, M. C.; Maynard, J. L.; Brasted, R. C. *Comprehensive Inorganic Chemistry*; D. Van Nostrand Co., Inc.: New York, 1954; Vol. 2, p 100.
43. Mukherji, A. K.; Sinha, A. K.; Dey, A. K. Complex Citrates of Metals in Inorganic Analysis: Some Preliminary Observations and the Application of Citrate Complex Formation in the Qualitative Analysis of the Metallic Ions of the Silver Group. *Anal. Chim. Acta* **1955**, *12*, 501–503.
44. Looney, B. B.; Denham, J. M. E.; Vangelas, K. M.; Bloom, N. S. Removal of Mercury from Low-Concentration Aqueous Streams Using Chemical Reduction and Air Stripping. *J. Environ. Eng.* **2003**, *129*, 819–825.
45. *WHO Guidelines for Drinking Water Quality*, 3rd ed.; **2004**; Vol. *1*.